

# Palladium Nanoparticles Confined in the Cages of MIL-101: An Efficient Catalyst for the One-Pot Indole Synthesis in Water

Hui Li,<sup>\*,†</sup> Zhonghong Zhu,<sup>†</sup> Fang Zhang,<sup>†</sup> Songhai Xie,<sup>‡</sup> Hexing Li,<sup>\*,†</sup> Ping Li,<sup>§</sup> and Xinggui Zhou<sup>§</sup>

<sup>†</sup>The Education Ministry Key Lab of Resource Chemistry and Shanghai Key Laboratory of Rare Earth Functional Materials, Shanghai Normal University, Shanghai 200234, P.R. China

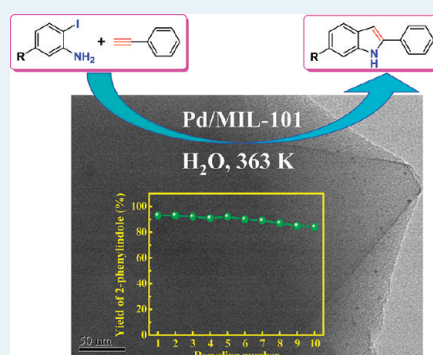
<sup>‡</sup>Department of Chemistry, Fudan University, Shanghai 200433, P.R. China

<sup>§</sup>State Key Laboratory of Chemical Engineering, East China University of Science and Technology, Shanghai 200237, P.R. China

**S** Supporting Information

**ABSTRACT:** A hydrothermally stable metal–organic framework, MIL-101, was used as support for a metallic Pd nanoparticle catalyst. With the characterization of X-ray photoelectron spectroscopy, X-ray diffraction, N<sub>2</sub> physisorption, scanning electron microscopy, transmission electron microscopy, and CO chemisorption, the resulting Pd nanoparticles were identified to be confined in the cages of MIL-101. During the one-pot indole synthesis between 2-iodoaniline and phenylacetylene in water, the as-prepared Pd catalyst was more active and stable than the metallic Pd nanoparticles supported on MCM-41. The enhanced catalytic properties were found to depend on both the texture and the surface chemistry of the MIL-101 support.

**KEYWORDS:** palladium, MOFs, domino indole synthesis, clean organic synthesis, water-medium



## INTRODUCTION

Indole nuclei occur widely in natural and pharmacological products as the building blocks and have unique biological activities.<sup>1</sup> Numerous synthetic strategies have been developed for their preparation in the past century.<sup>2–8</sup> Among them, the catalytic synthesis of indole ring systems through cycloadditions of 2-haloanilines with alkynes has proven to be the most powerful tool.<sup>9</sup> Generally, this reaction proceeds via an intermediate alkyne which then cyclizes in situ (Scheme 1). Because homogeneous palladium complexes can catalyze both the Sonogashira cross-coupling reaction and the subsequent ring-closure reaction,<sup>10–15</sup> they have been the most frequently employed for one-pot catalytic synthesis of indoles.<sup>16–19</sup> This one-pot process displays advantages in its lower costs mainly linked to separation and refining procedures;<sup>20–24</sup> however, homogeneous catalysis also presents a number of drawbacks, particularly including the catalyst reusability and the environmental pollution from heavy metallic ions.<sup>25–29</sup> Additionally, the reaction generally proceeds in organic solvents where Pd complexes can dissolve to form a homogeneous system, which also causes the recyclability problem of organic solvents.<sup>30</sup> The development of a heterogeneous Pd catalytic system in water-medium seems a promising option to address these problems. Recently, Djakovitch's group successfully used heterogeneous Pd loaded on activated carbon for one-pot indole synthesis.<sup>31,32</sup> Up to now, several heterogeneous Pd-containing systems had been developed for one-pot indole synthesis.<sup>33–37</sup> Although such heterogeneous catalyst was active during one-pot synthesis of 2-phenylindole, there is still space to enhance the reactivity of the Pd catalyst through increase of the

dispersion degree of the Pd active sites. Moreover, the problem resulting from the use of organic solvent had not been overcome completely despite the application of mixed DMF/H<sub>2</sub>O solvent (1:1). Therefore, a key issue for this study is to find an attractive support with high porosity and surface hydrophobicity, which can not only enhance the dispersion of Pd active sites but also allow for organic reactions performed in water.

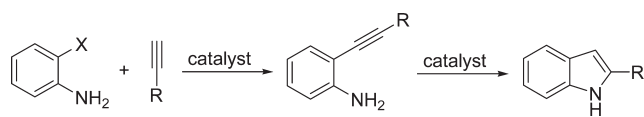
Presently, metal organic frameworks (MOFs) have attracted growing attention from both academia and industry owing to their outstanding features and thus specific applications, such as luminescence,<sup>38</sup> magnetic properties,<sup>39</sup> gas storage and adsorptive separation,<sup>40–42</sup> and catalytic properties.<sup>43–45</sup> In the domain of catalysis, besides the well-demonstrated catalytic activity of pure MOFs,<sup>46–53</sup> these materials are also attractive candidates for catalyst supports because of their unique porous features. Indeed, MOFs have been used as host matrixes to incorporate metal nanoparticles because their ultimately large surface area and narrow micropore distribution facilitate high metallic dispersion, which is of high interest for catalytic activity.<sup>54–66</sup> By an incipient wetness infiltration of Pd(acac)<sub>2</sub> (acac = acetylacetonate) precursor followed by reduction in hydrogen or under vacuum, Sabo et al. prepared Pd nanoparticles loaded on MOF-5 [Zn<sub>4</sub>O(bdc)<sub>3</sub>, bdc = benzene-1,4-dicarboxylate], which had been demonstrated to be a good catalyst for styrene hydrogenation.<sup>54</sup> However, the as-prepared Pd/MOF-5 is unstable in contact with water or

Received: July 8, 2011

Revised: October 5, 2011

Published: October 06, 2011

### Scheme 1. Catalytic Synthesis of Indole through Cycloaddition of 2-Haloanilines with Monosubstituted Alkyne



humid air because of the low hydrothermal stability of the MOF-5 support.<sup>54</sup> In 2005, Férey's group reported the synthesis and characterization of MIL-101 [Cr<sub>3</sub>F(H<sub>2</sub>O)<sub>2</sub>O(bdc)<sub>3</sub>],<sup>67</sup> which offers sufficient possibilities for application in heterogeneous catalysis because of its ultimately large specific surface area combined with a high crystallinity, mesoporous nature, and relatively high thermal and chemical stability in water. Using amine-grafted MIL-101 as support, Hwang et al. successfully encapsulated Pd nanoparticles by ionic reaction of ammonium groups with [PdCl<sub>4</sub>]<sup>2-</sup> and a subsequent reduction with sodium borohydride, which showed comparable reactivity with that of a commercial Pd/C catalyst during the Heck coupling reaction.<sup>53</sup> Henschel et al. prepared a hydrogenation catalyst, Pd/MIL-101, via incipient wetness impregnation, which is a more facile method for the incorporation of Pd nanoparticles into MIL-101 since no additional surface grafting of functional groups is needed to chelate palladium species.<sup>62</sup> El-Shall et al. developed an effective microwave-assisted chemical reduction approach to incorporating Pd nanoparticles into MIL-101, and compared the catalytic activity toward CO oxidation of embedded Pd nanoparticles with those loaded on the outer surface.<sup>63</sup> More recently, Pan et al. demonstrated that Pd@MIL-101 had enhanced catalytic efficiency in a one-step synthesis of methyl isobutyl ketone than Pd on traditional materials, such as metal oxides and zeolites.<sup>65</sup> Although the above-mentioned Pd/MIL-101 catalysts were investigated for catalytic activity and stability, to the best of our knowledge, their catalytic behavior in aqueous organic reaction has been rarely addressed so far.<sup>66</sup> As a class of organic–inorganic hybrid materials, MOFs are more hydrophobic relative to the traditional inorganic supports (silica, carbon, and alumina).<sup>68</sup> The enhanced surface hydrophobicity will be anticipated to increase the catalytic efficiency in aqueous organic reactions through enriching the organic substances on the catalyst surface,<sup>69</sup> which can open the door to green catalysis using water as replacing solvent in organic synthesis. In the present work, we embedded Pd nanoparticles within MIL-101 via a facile incipient wetting procedure followed by reduction with hydrogen. Their catalytic properties are evaluated in an atom-economy synthesis of indole in water which shows superior catalytic efficiency when compared to other catalysts, such as Pd/MCM-41 and commercial Pd/C. On the basis of various characterizations, the correlation of catalytic observations to the structural characteristics has been tentatively established.

## EXPERIMENTAL PROCEDURES

**Catalyst Preparation.** All of the chemicals used in this experiment were analytical grade and used without further purification. MIL-101 was synthesized following the method reported by Férey et al.<sup>67</sup> The supported Pd samples were prepared according to the procedure described as follows: first, 7.1 mg Pd(acac)<sub>2</sub> was dissolved into 0.30 mL of chloroform. A calculated amount of activated MIL-101 was then impregnated

with the Pd precursor solution. The mixture was stirred vigorously for 3 h in Argon flow. After being dried at 423 K for 4 h, the impregnated MIL-101 samples were reduced in a 10% H<sub>2</sub>/Ar flow at 493 K for 2 h. The as-prepared samples were designated as x%-Pd/MIL-101, where x% denotes the nominal Pd loading. For comparison, the reference 3%-Pd/MCM-41 catalyst was prepared through the same incipient wet impregnation followed by the reduction method.

**Catalyst Characterization.** The bulk composition and Pd loading were analyzed by means of inductively coupled plasma (ICP; Varian VISTA-MPX). The crystalline structure was determined by X-ray diffraction (XRD; Rigaku D/Max-RB with Cu K $\alpha$  radiation). The catalyst shapes and morphologies were observed by both field emission scanning electron microscopy (FESEM; HITACHI S-4800) and transmission electron microscopy (TEM; JEOL JEM2100). The location of Pd nanoparticles within the framework of MIL-101 support was determined by high-angle annular dark-field scanning transmission electron microscopy (HAADF-STEM; JEOL JEM2100F). The surface electronic states were investigated by X-ray photoelectron spectroscopy (XPS; ULVAC-PHI PHI5000 VersaProbe using Al K $\alpha$  radiation). All of the binding energy (BE) values were calibrated by using C 1s = 284.6 eV as a reference. N<sub>2</sub> adsorption–desorption isotherms were obtained at 77 K using a Quantachrome NOVA 4000e apparatus. By N<sub>2</sub> adsorption, the Brunauer–Emmett–Teller (BET) surface area ( $S_{\text{BET}}$ ) was calculated by using the multiple-point BET method in the relative pressure range of  $P/P_0 = 0.05–0.2$ . The pore volume and pore size distribution curve were obtained by the Barrett–Joyner–Halenda model. The active surface area ( $S_{\text{act}}$ ) was measured by the CO chemisorption at room temperature, which was performed on a Micromeritics AutoChem II 2920 instrument using a dynamic pulse method. The sample was purged under an argon flow (purity of 99.997%, treated with an Alltech Oxy-Trap column) at 423 K for 2 h. The pretreated sample was cooled down to room temperature under argon atmosphere, and CO pulses were injected at 303 K until the calculated areas of consecutive pulses were constant. According to the CO chemisorption,  $S_{\text{act}}$  of the as-prepared catalyst was calculated assuming Pd/CO = 1 and a Pd surface density of  $1.27 \times 10^{19}$  atoms m<sup>-2</sup>. Every sample was measured three times. The reproducibility of the results was checked by repeating the measurements three times on the same catalyst and was found to be within acceptable limits ( $\pm 2\%$ ).

**Activity Test.** In a typical experiment, 2-iodoaniline (1.0 mmol) and phenylacetylene (1.2 mmol) were added into water (10 mL). To this were added catalyst (containing 0.01 mmol Pd), PPh<sub>3</sub> (0.02 mmol), CuI (0.05 mmol), and K<sub>2</sub>CO<sub>3</sub> (1.5 mmol), and the mixture was stirred at 363 K under argon. Reaction samples were taken at regular intervals and monitored by GC-MS (Agilent 6890n-5973i equipped with a DB-5 capillary column), from which the conversion of 2-iodoaniline and the yield of 2-phenylindole were calculated. For the recycling test, the recovered catalyst was further washed sufficiently with ethanol followed by water.

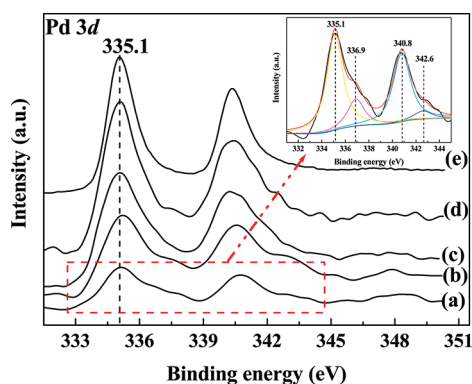
## RESULTS AND DISCUSSION

**Characterization of the Catalysts.** ICP analysis reveals that the Pd loadings in all the Pd-containing samples were very similar to the nominal Pd loadings in the preparation precursors (see Table 1). XPS spectra (Figure 1) demonstrate that almost all the Pd species in all the Pd-containing samples except 1%-Pd/MIL-101 and

**Table 1.** Some Structural Properties of the As-Prepared Pd-Based Catalysts

sample	Pd loading (wt %)	$S_{\text{Pd}}$ ( $\text{m}^2/\text{g}$ )	$d_{\text{Pd}}^a$ (nm)
1%-Pd/MIL-101	0.96	$144 \pm 2.6$	3.5
2%-Pd/MIL-101	2.0	$156 \pm 2.1$	3.2
3%-Pd/MIL-101	2.9	$191 \pm 1.2$	2.6
4%-Pd/MIL-101	3.8	$165 \pm 2.1$	3.0
3%-Pd/MCM-41	2.8	$127 \pm 1.5$	3.9

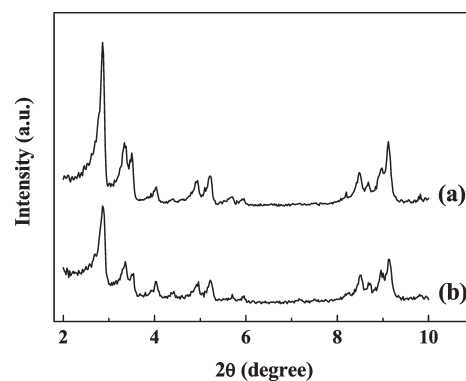
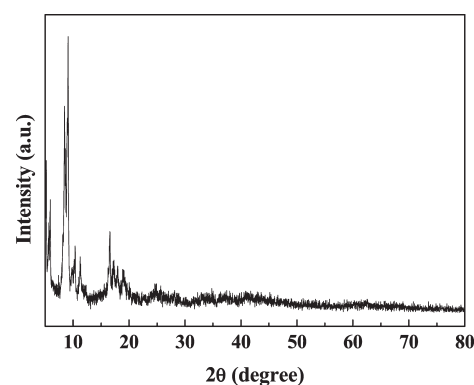
<sup>a</sup> Calculated as  $6/(\rho S_{\text{Pd}})$ ,  $\rho = 12.02 \text{ g/cm}^3$ .

**Figure 1.** XPS of (a) 1%-Pd/MIL-101, (b) 2%-Pd/MIL-101, (c) 3%-Pd/MIL-101, (d) 4%-Pd/MIL-101, and (e) 3%-Pd/MCM-41. The inset is the peak separation of Pd 3d level for (a).

2%-Pd/MIL-101 were present in the metallic state with the BE about 335.1 eV in the Pd  $3d_{5/2}$  core level.<sup>70</sup> The presence of PdO species in 1%-Pd/MIL-101 was confirmed by fitting the high-energy shoulder on the metallic Pd lines at BE of about 336.9 and 342.6 eV (inset in Figure 1).<sup>71</sup> For 2%-Pd/MIL-101, the amount of oxidized Pd species is much lower than 1%-Pd/MIL-101 (Figure 1b). The production of oxidized Pd species could be due to the oxidation of metallic Pd left in an oxygen-containing environment.<sup>72,73</sup> XPS analyses of 1%-Pd/MIL-101 and 2%-Pd/MIL-101 were also performed after in situ treatment in a 10%  $\text{H}_2/\text{Ar}$  flow at 493 K for 2 h. It was found that no significant PdO species could be observed over both samples after such treatment (Supporting Information, Figure S1), which further demonstrated that the presence of oxidized Pd species was due to the exposure of metallic Pd to air.

The low-angle XRD pattern of the as-prepared MIL-101 (Figure 2a) is in excellent agreement with the simulated pattern reported by Férey et al.<sup>67</sup> The almost unchanged XRD pattern of 3%-Pd/MIL-101 (Figure 2b) shows that the Pd incorporation occurred with no apparent loss of structure integrity, but with some slight variations of the Bragg intensities. Furthermore, no significant diffraction peak characteristic of Pd species is detected from the wide-angle XRD pattern for 3%-Pd/MIL-101 (Figure 3), which might be related to the embedding of Pd nanoparticles into the pores of MIL-101. This observation is very similar to the results reported by El-Shall et al.,<sup>63</sup> where the incorporation of Pd in MIL-101 produced hardly significant signals of Pd in the XRD pattern unless the Pd loading was more than 4.9 wt %.

The  $\text{N}_2$  adsorption–desorption isotherms and the pore size distribution profiles of the as-prepared MIL-101 and 3%-Pd/MIL-101 are shown in Figure 4. The  $S_{\text{BET}}$  and total pore volume of MIL-101 were calculated to be  $3820 \text{ m}^2 \text{ g}^{-1}$  and  $1.86 \text{ cm}^3 \text{ g}^{-1}$ ,

**Figure 2.** Low-angle XRD patterns of (a) MIL-101, and (b) 3%-Pd/MIL-101.**Figure 3.** Wide-angle XRD pattern of 3%-Pd/MIL-101.

respectively, which are close to the reported values.<sup>52,63,65,67</sup> The isotherms of MIL-101 have secondary uptakes around  $P/P_0 = 0.1$  and 0.2 (Figure 4a), indicating the existence of two kinds of nanopores.<sup>52</sup> The pore size distribution curve of MIL-101 also displays two different pore sizes, 1.7 and 2.2 nm (Figure 4b), which are similar to the results reported recently by Hwang et al.<sup>53</sup> and Pan et al.<sup>65</sup> Compared with the bare MIL-101,  $S_{\text{BET}}$  and pore volume of 3%-Pd/MIL-101 decreased to  $3200 \text{ m}^2 \text{ g}^{-1}$  and  $1.58 \text{ cm}^3 \text{ g}^{-1}$ , respectively, mainly because of the occupation of the cages of MIL-101 by the monodisperse Pd nanoparticles. Meanwhile, the incorporation of Pd also led to a slight decrease of the pore sizes (Figure 4b).

As shown in FESEM image (Figure 5a), the as-prepared MIL-101 is on the micrometer scale, which is similar to the previous reports.<sup>52,63</sup> From the TEM image of the as-prepared MIL-101 (Figure 5b), the cubic symmetry of the bare MIL-101 is also reflected in the shape of the crystals. In Figure 5b, we could also observe well-defined MIL-101 crystalline with highly ordered two-dimensional porous structures. The angle between vector A and B with same  $d$  spacing ( $d_A = d_B = 4.9 \text{ nm}$ ) is about  $70.5^\circ$ , which could be indexed as the zone axis  $[110]$  of MIL-101.<sup>74</sup> The vector A and B are  $(1\bar{1}\bar{1})$  and  $(1\bar{1}\bar{1})$ , respectively. TEM image of 3%-Pd/MIL-101 (Figure 5c) reveals similar morphology and pore structure to the bare MIL-101, demonstrating that the structural integrity of MIL-101 was preserved after the Pd incorporation. In this image, only a few particles appear on the surface of MIL-101. It is important to note that the high-resolution TEM (HRTEM) image was taken in the shortest

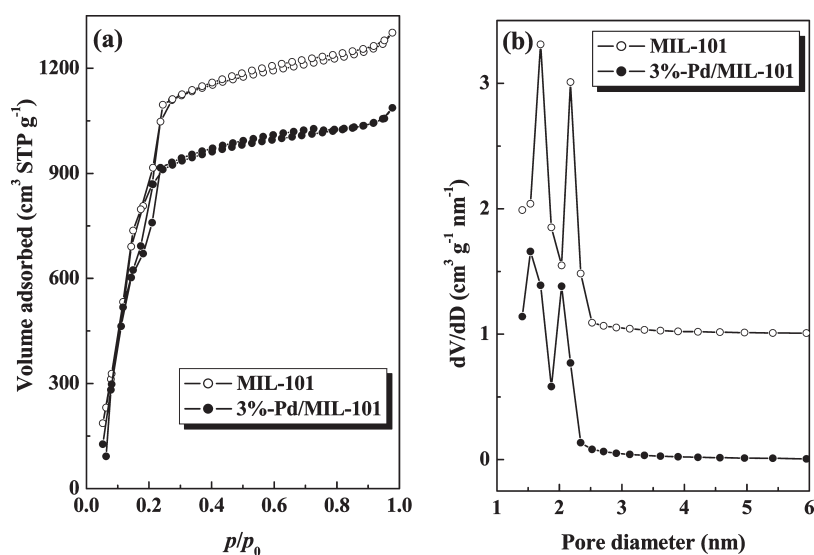


Figure 4. (a) N<sub>2</sub> adsorption–desorption isotherms and (b) pore size distributions of MIL-101 and 3%-Pd/MIL-101.

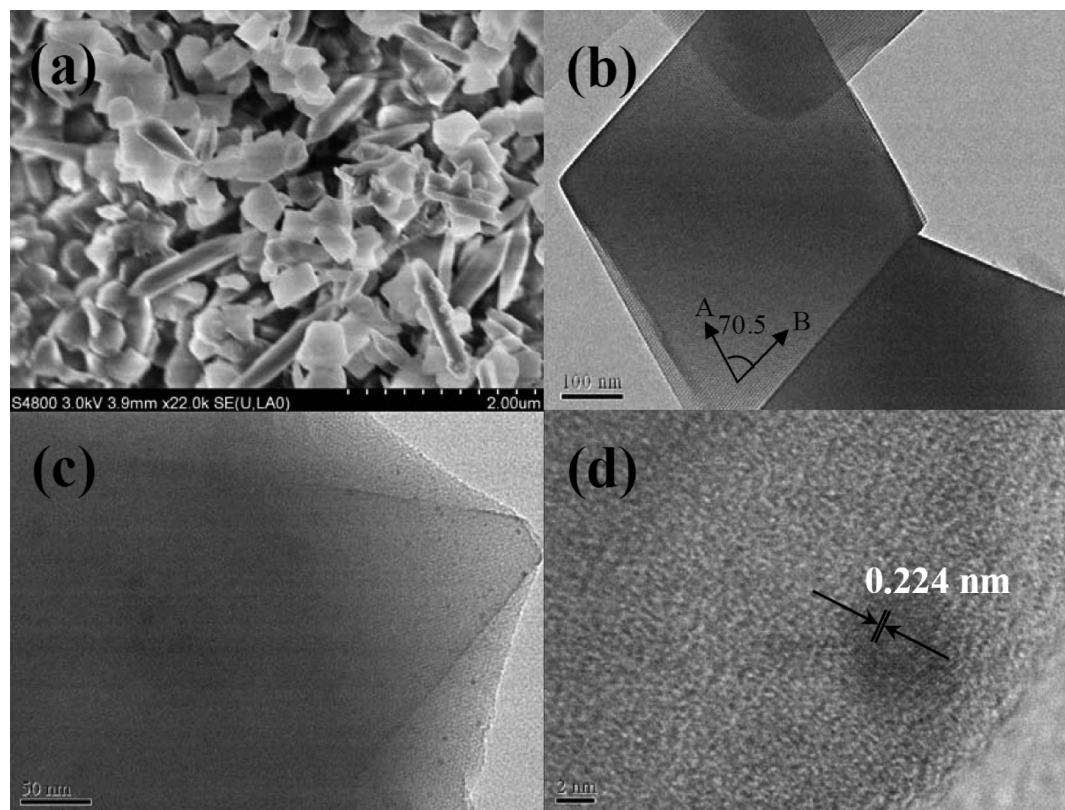
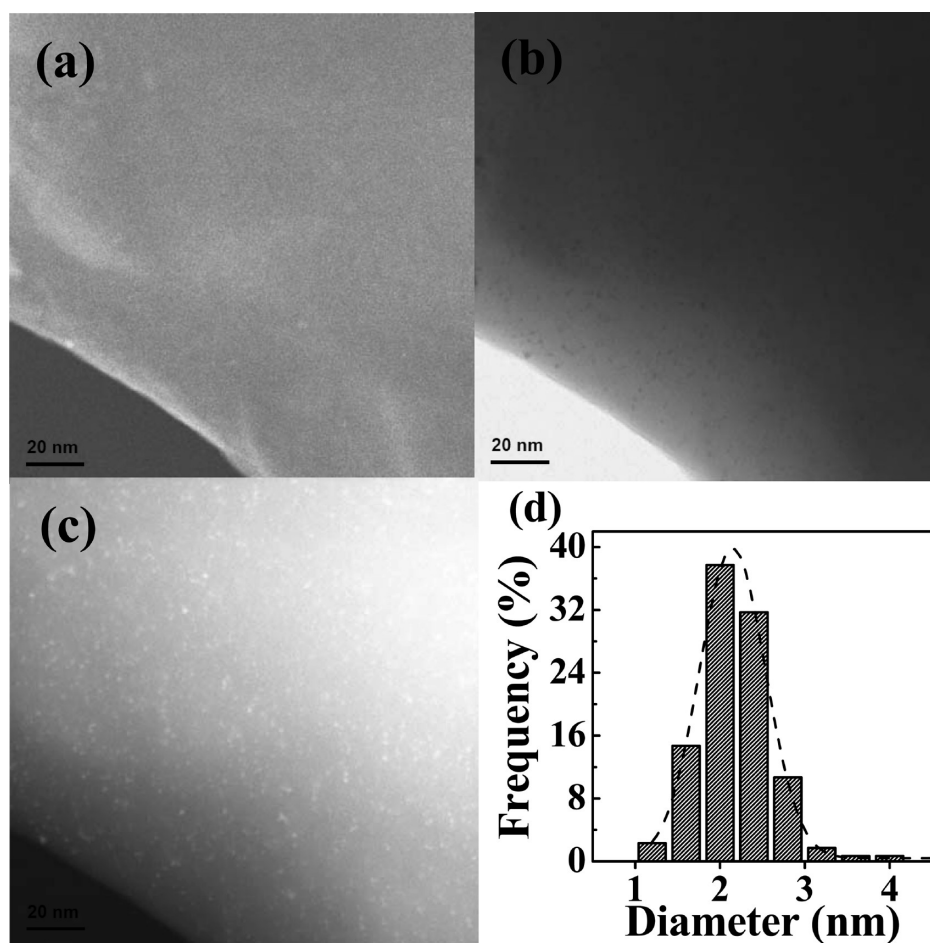


Figure 5. (a) SEM and (b) TEM images of MIL-101, (c) TEM and (d) HRTEM images of 3%-Pd/MIL-101.

possible time because MIL-101 is extremely sensitive to the electron beam and, in usual conditions, the structure collapses after a few minutes.<sup>74</sup> Despite the distorted HRTEM image (Figure 5d), it suggested that the particles located outside MIL-101 had a typical face-centered cubic (fcc) Pd structure, which corresponded to a Pd (111) interplanar spacing of 0.224 nm.<sup>75</sup> This observation indicated that most of the Pd nanoparticles actually inserted within the MIL-101 crystals, which is in clear

contrast to the result of 3%-Pd/MCM-41 where a portion of Pd particles were located at the external surface (Supporting Information, Figure S2).

It is difficult to estimate the Pd dispersion when obtaining accurate Pd crystallite size distribution histograms from TEM micrographs because of the poor particle-support contrast when particles are embedded in the cages of MIL-101. Thus, we used CO chemisorption to measure the Pd particle size,<sup>76</sup> and this



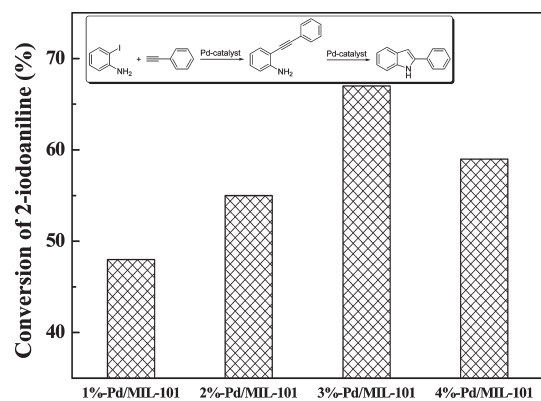
**Figure 6.** STEM images of 3%-Pd/MIL-101 catalyst: (a) SE, (b) STEM-BF, and (c) STEM-DF modes. (d) The corresponding particle size distribution histogram.

technique offers reproducible results (shown in Table 1). For x%-Pd/MIL-101, the metal dispersion degree increased first and then decreased with the increase of Pd loading. The maximum  $S_{Pd}$  was obtained at 3%-Pd/MIL-101. The decrease in  $S_{Pd}$  with the increase of Pd loading is reasonable; however, the  $S_{Pd}$  of 1%-Pd/MIL-101 and 2%-Pd/MIL-101 calculated on the basis of total Pd weight is lower than 3%-Pd/MIL-101. The reason for such abnormality is that 1%-Pd/MIL-101 and 2%-Pd/MIL-101 contain much more oxidized Pd, as confirmed by the XPS analysis. Comparing to the results in Table 1, it is observed that 3%-Pd/MIL-101 had much higher Pd dispersion degree than 3%-Pd/MCM-41 regardless of nearly the same Pd loading. It can also be concluded that most of the Pd particles in 3%-Pd/MIL-101 are confined in the cages of MIL-101 because the mean diameter of Pd particles (2.6 nm) is slightly larger than the pore diameters of MIL-101.<sup>65</sup> However, for 3%-Pd/MCM-41, the measured Pd diameter (3.9 nm) is much larger than the pore size of MCM-41 (2.4 nm), suggesting that most of Pd particles aggregated on the outer surface of MCM-41 support.

To further confirm the embedding of Pd nanoparticles within the cages of MIL-101, some images were obtained by HAADF-STEM for the 3%-Pd/MIL-101 catalyst, which was recorded in SE (Secondary electron), STEM-BF (STEM Bright-Field) and STEM-DF (STEM Dark-Field) modes, respectively (Figure 6). The SE mode could only show the surface morphology (5–10 nm depth)

and STEM-BF mode exhibits the projection of both surface and inner structure information. The STEM-DF mode could enhance the contrast of heavy metal atoms by collecting the high-angle incoherent scattering signals, which confirmed the information of the STEM-BF mode. The three images at same position clearly demonstrated the locations and distribution of Pd nanoparticles. Generally, the particles on the surface are really unavoidable; however, only a few of the particles are found on the surface and many nanoparticles are monodispersed at the inner space. The average particle size is around 2.1 nm (Figure 6d) which could be attributed to the limitation of mesopores of MIL-101. Accordingly, even though we could not record the channel with clusters simultaneously, the HAADF-STEM observations strongly support that the locations of the Pd nanoparticles are inside the cages of MIL-101.

The combined results from  $N_2$  physisorption, TEM, CO chemisorption characteristics, and HAADF-STEM demonstrated the existence of Pd nanoparticles within the cages of MIL-101, which is most likely relative to the special structure of the host material.<sup>63,64</sup> First, the very large surface area of the as-prepared MIL-101 is favorable for the dispersion of Pd active sites. Second, the presence of an organic moiety in MIL-101 could also improve the Pd particle distribution owing to the isolating effect of the hydrophobic groups,<sup>77</sup> which can inhibit the migration and agglomeration of the Pd ions and Pd particles



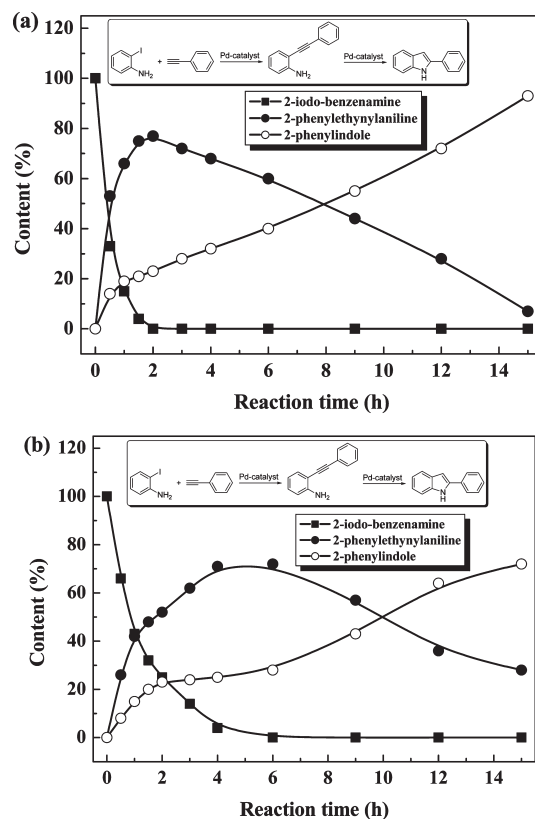
**Figure 7.** Conversion of 2-iodoaniline obtained on x%-Pd/MIL-101. Reaction conditions: 2-iodoaniline (1.0 mmol), phenylacetylene (1.2 mmol), PPh<sub>3</sub> (0.02 mmol), CuI (0.05 mmol), K<sub>2</sub>CO<sub>3</sub> (1.5 mmol), H<sub>2</sub>O (10 mL), and Pd/MIL-101 (1.0 mol % Pd), *T* = 363 K, *t* = 0.5 h.

during the drying and preparation processes. Third, the presence of monodisperse pores have a confinement effect on the growth and gathering of Pd particles in the cages.<sup>67</sup> Once the Pd precursors were introduced into the cages, the growth of Pd particles during the reduction process would be confined by the pores with fixed dimension, leading to monodisperse Pd particles on the scale of 1 to 3 nm.<sup>63,64</sup> Because MCM-41 material possesses straight channels, there was no remarkable confinement effect. As a result, a portion of the formed Pd particles might emigrate out the pore channels of MCM-41, and agglomerate on the outer surface.

**Catalytic Performances.** Both the crystallinity and the framework integrity of MIL-101 are very stable, and can be well preserved even after being treated in water at 373 K for 48 h (Supporting Information, Figure S3–S5). Additionally, this hybrid solid is more hydrophobic than the traditionally used pure inorganic supports,<sup>61</sup> facilitating the enrichment and adsorption of organic substances on the catalyst in aqueous solution. These properties present the opportunities for using this material in aqueous organic reactions.

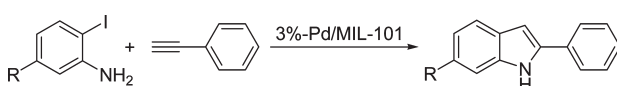
The as-prepared Pd-based catalysts were subjected to one-pot synthesis of indole between 2-haloaniline and monosubstituted alkyne in water. We first tested the catalytic activity of x%-Pd/MIL-101 for the reaction between 2-iodoaniline and phenylacetylene using the same amount of Pd to investigate the influence of Pd loading on catalytic activity. Preliminary study revealed that the maximum 2-iodoaniline conversion was obtained on 3%-Pd/MIL-101 (Figure 7). Obviously, the highest reactivity over 3%-Pd/MIL-101 may be attributed to its highest *S*<sub>Pd</sub> (Table 1). The 3%-Pd/MIL-101 was therefore selected for the following studies.

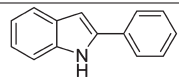
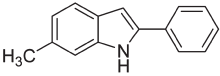
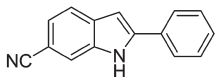
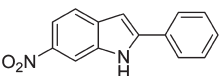
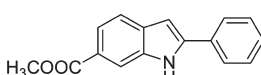
Figure 8 showed the reaction profile of reaction of 2-iodoaniline and phenylacetylene over 3%-Pd/MIL-101 and 3%-Pd/MCM-41. The intermediate compound 2-phenylethynylaniline resulting from the Sonogashira C–C coupling reaction between 2-iodoaniline and phenylacetylene could be observed in these experiments, which revealed that the present indole synthesis reaction is a consecutive reaction, as previously reported in the literature.<sup>7,8,31,32,36</sup> Despite similar Pd loading, 3%-Pd/MIL-101 was much more active than 3%-Pd/MCM-41 (Figure 8), since complete conversion of 2-iodoaniline was achieved within 2 h over the former while 4 h was needed to convert 2-iodoaniline completely over the latter. This should be mainly attributed to the larger number of Pd active sites in 3%-Pd/MIL-101 relative to 3%-Pd/MCM-41 (see *S*<sub>Pd</sub> values in Table 1), which would



**Figure 8.** Reaction profiles of 2-iodoaniline and phenylacetylene over (a) 3%-Pd/MIL-101 and (b) 3%-Pd/MCM-41. Reaction conditions: 2-iodoaniline (1.0 mmol), phenylacetylene (1.2 mmol), PPh<sub>3</sub> (0.02 mmol), CuI (0.05 mmol), K<sub>2</sub>CO<sub>3</sub> (1.5 mmol), H<sub>2</sub>O (10 mL), and Pd/MIL-101 (1.0 mol % Pd), *T* = 363 K.

allow more favorable oxidative addition of the metallic Pd to the carbon–halogen bond, and therefore obtain more efficient catalyst.<sup>78</sup> Additionally, the 2-iodoaniline conversions within 0.5 h were 67% and 34% over 3%-Pd/MIL-101 and 3%-Pd/MCM-41, respectively. Thus, the initial reaction rate over 3%-Pd/MIL-101 was 2.0 times of that over 3%-Pd/MCM-41. Because the *S*<sub>Pd</sub> of 3%-Pd/MIL-101 was 1.5 times of that of 3%-Pd/MCM-41, we can conclude that the larger *S*<sub>Pd</sub> of 3%-Pd/MIL-101 was not the only factor responsible for its higher activity. Obviously, the enhanced surface hydrophobicity<sup>68</sup> and the existence of Lewis acidity<sup>66</sup> on MIL-101 owing to the organic linkers (bdc) and the open metal (Cr<sup>3+</sup>) sites would favor the adsorption of 2-iodoaniline, and thus enhance the reactivity of 3%-Pd/MIL-101. From Figure 8a, it can be clearly seen that the conversion of 2-iodoaniline increased almost linearly with the reaction time over 3%-Pd/MIL-101, indicating that the adsorption for 2-iodoaniline on MIL-101 reached surface saturation. A deviation from the straight line was observed when the 2-iodoaniline conversion was more than 85%, possibly because of the extremely low 2-iodoaniline concentration. However, for 3%-Pd/MCM-41, no linear increase of 2-iodoaniline conversion with the reaction time could be observed (Figure 8b). The obtained ln(1-conversion) increased linearly with the reaction time (Supporting Information, Figure S6), implying the present reaction was first-order with respect to 2-iodoaniline over 3%-Pd/MCM-41. This result suggested that the adsorption for 2-iodoaniline over 3%-Pd/MCM-41 could not reach surface

**Table 2.** 3%-Pd/MIL-101 Catalyzed One-Pot Indole Synthesis Reactions<sup>a</sup>


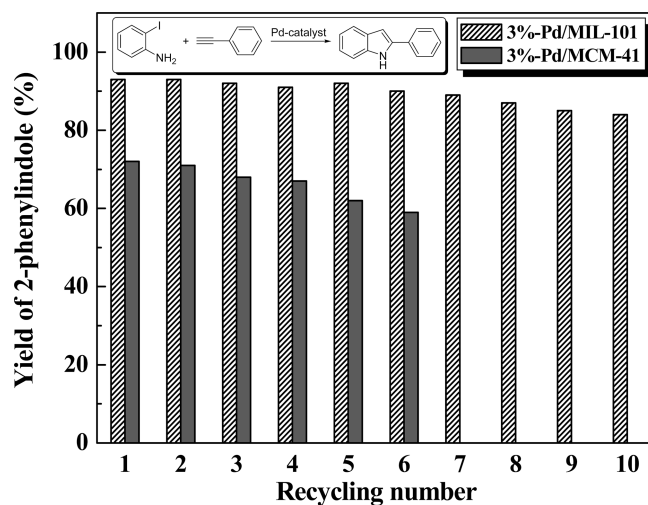
Entry	R	Product	Yield <sup>b</sup> (%)
1	H-		93
2	CH <sub>3</sub> -		89
3	CN-		98
4	NO <sub>2</sub> -		98
5	CH <sub>3</sub> COO-		97

<sup>a</sup> Reaction conditions: 2-iodoaniline (1.0 mmol), phenylacetylene (1.2 mmol), PPh<sub>3</sub> (0.02 mmol), CuI (0.05 mmol), K<sub>2</sub>CO<sub>3</sub> (1.5 mmol), H<sub>2</sub>O (10 mL), and Pd/MIL-101 (1.0 mol % Pd), *T* = 363 K, *t* = 15 h. <sup>b</sup> Determined by GC analysis.

saturation at the present concentration because of the weaker adsorption of 2-iodoaniline on MCM-41 in comparison with MIL-101. After reaction for 15 h, an excellent 93% yield of 2-phenylindole could be obtained over 3%-Pd/MIL-101 (entry 1 in Table 2). However, in comparison with Pd/C reported by Djakovitch's group (72% yield at 393 K in 6 h),<sup>32</sup> 3%-Pd/MIL-101 (40% yield at 363 K in 6 h) showed lower activity. This is clearly due to the lower reaction temperature in this study than that used previously. For comparison, a commercial Pd/C catalyst (3 wt % Pd loading) was measured under the same reaction conditions, and only 25% yield of 2-phenylindole was achieved using Pd/C in the reaction between 2-iodoaniline and phenylacetylene in 6 h. The XPS analysis (Supporting Information, Figure S7a) reveals that all Pd species in the commercial Pd/C were present in metallic state. Meanwhile, both the TEM image (Supporting Information, Figure S7b) and the XRD pattern (Supporting Information, Figure S7c) demonstrated that the metallic Pd is present in the form of spherical particles with average size of more than 5 nm. Thus, one could conclude that the superior activity of 3%-Pd/MIL-101 to the commercial Pd/C was mainly due to the highly dispersed Pd active sites originating from the confinement effect of the cages of MIL-101 on the Pd nanoparticles.

3%-Pd/MIL-101 was also an active catalyst for the one-pot indole synthesis reaction between various 2-iodoanilines and phenylacetylene. The reactants of 2-iodoaniline with an electron-withdrawing or electron-donating group showed obvious difference in reactivity (entries 2–5 in Table 2), indicating that such reaction was sensitive to the electronic characteristics of the substituent under the present reaction conditions.

3%-Pd/MIL-101 could be easily separated from the reaction solution via centrifugation and could be used at least for 10 times during the one-pot aqueous indole synthesis reaction between 2-iodoaniline and phenylacetylene (Figure 9), showing its



**Figure 9.** Recycling tests of 3%-Pd/MIL-101 and 3%-Pd/MCM-41. Reaction conditions: 2-iodoaniline (1.0 mmol), phenylacetylene (1.2 mmol), PPh<sub>3</sub> (0.02 mmol), CuI (0.05 mmol), K<sub>2</sub>CO<sub>3</sub> (1.5 mmol), H<sub>2</sub>O (10 mL), and Pd/MIL-101 (1.0 mol % Pd), *T* = 363 K, *t* = 15 h.

superiority over the homogeneous catalysts. XPS analysis of the reused 3%-Pd/MIL-101 (Supporting Information, Figure S8a) indicated the no oxidation of metallic Pd occurred during the recycling test. Meanwhile, TEM image (Supporting Information, Figure S9a) showed that the morphology and pore structure of 3%-Pd/MIL-101 was mostly retained after 10 catalytic cycles. The catalyst weight decreased slightly after 10 consecutive runs, and no leaching of Pd could be determined by ICP analysis in the reaction mixtures during repetitive runs. The detection limit of Pd in the aqueous phase is determined as  $9 \times 10^{-4}$  mg/L in the present ICP analysis. Therefore, during the recycling test, the Pd content in the solution is less than 0.9 ppb. We thus argue that the weight loss of catalyst during the separation process, rather than the leaching of Pd species from 3%-Pd/MIL-101, was the main factor responsible for the slight decrease of the 2-phenylindole yield during the recycling tests. 3%-Pd/MCM-41 displayed a significant loss of reactivity (>20%) after being used repetitively for 6 times. Similarly, no significant PdO species could be observed over the reused 3%-Pd/MCM-41 (Supporting Information, Figure S8b), and only slight weight loss of 3%-Pd/MCM-41 after 6 consecutive runs was determined, while no leaching of Pd could be detected in the reaction mixtures for 3%-Pd/MCM-41 during repetitive uses. These implied that there existed other reason for the deactivation of 3%-Pd/MCM-41 during recycling tests. TEM morphology (Supporting Information, Figure S9b) revealed that the deactivation of 3%-Pd/MCM-41 could be mainly due to severe collapse of the pore structure of MCM-41 support and agglomeration of Pd nanoparticles. In contrast, because of the robust hydrothermal stability of the MIL-101 matrix and the confinement effect of the cages of MIL-101, the Pd nanoparticles in MIL-101 are durable during the reaction. According to this observation, the high durability of 3%-Pd/MIL-101 should be attributed to the special structure of MIL-101 which retards the agglomeration of Pd nanoparticles during the reaction.

## CONCLUSIONS

In summary, palladium nanoparticles (<3 nm) confined in the cages of MIL-101 could be employed as a catalyst for the domino

synthesis of indole in water, and exhibited enhanced efficiency relative to Pd/MCM-41 because of the special pore structure, the enhanced surface hydrophobicity, and the existence of Lewis acidity on of MIL-101. Meanwhile, the Pd/MIL-101 catalyst possessed better stability and could be used repetitively for at least 10 times, showing good potential for practical application. Our findings demonstrate the advantages of MIL-101 as support for metal nanoparticle catalysts in water-medium clean organic synthesis.

## ■ ASSOCIATED CONTENT

**S Supporting Information.** XPS of 1%-Pd/MIL-101 and 2%-Pd/MIL-101 after in situ treatment in a 10% H<sub>2</sub>/Ar flow at 493 K for 2 h, 3%-Pd/C catalyst, 3%-Pd/MIL-101 after 10 consecutive runs, as well as 3%-Pd/MCM-41 after 6 consecutive runs; TEM images of fresh 3%-Pd/MCM-41 and 3%-Pd/MCM-41 after 6 consecutive runs, 3%-Pd/C catalyst, and 3%-Pd/MIL-101 after 10 consecutive runs; time–ln(1–conversion) curve during the reaction between 2-iodoaniline and phenylacetylene over 3%-Pd/MCM-41; XRD pattern of 3%-Pd/C catalyst; low-angle XRD patterns, N<sub>2</sub> adsorption–desorption isotherms, pore size distributions, and TEM images of MIL-101 after hydrothermal treating. This material is available free of charge via the Internet at <http://pubs.acs.org>.

## ■ AUTHOR INFORMATION

### Corresponding Author

\*Phone: +86-21-64322272. Fax: +86-21-64322272. E-mail: [lihui@shnu.edu.cn](mailto:lihui@shnu.edu.cn) (Hu.L.), [hexing-li@shnu.edu.cn](mailto:hexing-li@shnu.edu.cn) (He.L.).

### Funding Sources

This work is supported by the National Natural Science Foundation of China (20973113, 20703011, 21107071), the 973 Program (2009CB226106), Shanghai Government (09JC1411400, 10SG41, S30406, 12YZ084, 09ZR1402300, 10PJ1408200, 11YZ88), and State Key Laboratory of Chemical Engineering (SKL-ChE-09C03).

## ■ REFERENCES

- (1) Somei, M.; Yamada, F. *Nat. Prod. Rep.* **2005**, *22*, 73.
- (2) Brown, R. K. In *Synthesis of the indole nucleus*; Houlihan, W. J., Ed.; Wiley-Interscience: New York, 1972; Part I.
- (3) Cacchi, S.; Fabrizi, G. *Chem. Rev.* **2005**, *105*, 2873.
- (4) Humphrey, G. R.; Kuethe, J. T. *Chem. Rev.* **2006**, *106*, 2875.
- (5) Patil, N. T.; Yamamoto, Y. *Chem. Rev.* **2008**, *108*, 3395.
- (6) Cacchi, S.; Fabrizi, G. *Chem. Rev.* **2010**, *111*, PR215.
- (7) Djakovitch, L.; Batail, N.; Genelot, M. *Molecules* **2011**, *16*, 5241.
- (8) Batail, N.; Genelot, M.; Dufaud, V.; Joucla, L.; Djakovitch, L. *Catal. Today* **2011**, *173*, 2.
- (9) Krüger, K.; Tillack, A.; Beller, M. *Adv. Synth. Catal.* **2008**, *350*, 2153.
- (10) Sonogashira, K.; Tohda, Y.; Hagihara, N. *Tetrahedron Lett.* **1975**, *16*, 4467.
- (11) Sonogashira, K. In *Comprehensive Organic Synthesis*; Trost, B. M., Fleming, I., Eds.; Pergamon Press: Oxford, U.K., 1991; Vol. 3, pp 521–549.
- (12) Sonogashira, K. In *Metal-Catalyzed Cross-Coupling Reactions*; Diederich, F., Stang, P. J., Eds.; Wiley-VCH: Weinheim, Germany, 1998; pp 203–229.
- (13) Sonogashira, K. In *Handbook of Organopalladium Chemistry for Organic Synthesis*; Negishi, E., de Meijere, A., Eds.; Wiley-Interscience: New York, 2002; pp 493–529.
- (14) Sonogashira, K. *J. Organomet. Chem.* **2002**, *653*, 46.
- (15) Chinchilla, R.; Nájera, C. *Chem. Rev.* **2007**, *107*, 874.
- (16) Iritani, K.; Matsubara, S.; Utimoto, K. *Tetrahedron Lett.* **1988**, *29*, 1799.
- (17) Rudisill, D. E.; Stille, J. K. *J. Org. Chem.* **1989**, *54*, 5856.
- (18) Sun, L. P.; Huang, X. H.; Dai, W. M. *Tetrahedron* **2004**, *60*, 10983.
- (19) Zeni, G.; Larock, R. C. *Chem. Rev.* **2004**, *104*, 2285.
- (20) Larock, R. C.; Yum, E. K. *J. Am. Chem. Soc.* **1991**, *113*, 6689.
- (21) Ezquerro, J.; Pedregal, C.; Lamas, J. M.; Barluenga, J.; Perez, M.; Garcia-Martin, M. A.; Gonzalez, J. M. *J. Org. Chem.* **1996**, *61*, 5804.
- (22) Fagnola, M. C.; Candiani, I.; Visentin, G.; Cabri, W.; Zarini, F.; Mongelli, N.; Bedeschi, A. *Tetrahedron Lett.* **1997**, *38*, 2307.
- (23) Witulski, B.; Alayrac, C.; Tevzadze-Saefel, L. *Angew. Chem., Int. Ed.* **2003**, *42*, 4257.
- (24) Sakai, H.; Tsutsumi, K.; Morimoto, T.; Kakiuchi, K. *Adv. Synth. Catal.* **2009**, *350*, 2498.
- (25) Bhanage, B.; Arai, M. *Catal. Rev.* **2001**, *43*, 315.
- (26) de Vries, J. G. *Can. J. Chem.* **2001**, *79*, 1086.
- (27) Tucker, C. E.; de Vrie, J. G. *Top. Catal.* **2002**, *19*, 111.
- (28) Garrett, C. E.; Prasad, K. *Adv. Synth. Catal.* **2004**, *346*, 889.
- (29) Welch, C. J.; Albaneze-Walker, J.; Leonard, W. R.; Biba, M.; DaSilva, J.; Henderson, D.; Laing, B.; Mathre, D. J.; Spencer, S.; Bu, X.; Wang, T. *Org. Process Res. Dev.* **2005**, *9*, 198.
- (30) Li, C. J.; Chan, T. H. *Comprehensive Organic Reactions in Aqueous Media*, 2nd ed.; Wiley-Interscience: New York, 2007.
- (31) Chouzier, S.; Gruber, M.; Djakovitch, L. *J. Mol. Catal. A: Chem.* **2004**, *212*, 43.
- (32) Gruber, M.; Chouzier, S.; Koehler, K.; Djakovitch, L. *Appl. Catal., A* **2004**, *265*, 161.
- (33) Djakovitch, L.; Rollet, P. *Adv. Synth. Catal.* **2004**, *346*, 1782.
- (34) Pal, M.; Subramanian, V.; Batchu, V. R.; Dager, I. *Synlett* **2004**, 1965.
- (35) Hong, K. B.; Lee, C. W.; Yum, E. K. *Tetrahedron Lett.* **2004**, *45*, 693.
- (36) Djakovitch, L.; Dufaud, V.; Zaidi, R. *Adv. Synth. Catal.* **2006**, *348*, 715.
- (37) Layek, M.; Lakshmi, U.; Kalita, D.; Barange, D. K.; Islam, A.; Mukkanti, K.; Pal, M. *Beilstein J. Org. Chem.* **2009**, *5*, No. 46.
- (38) Allendorf, M. D.; Bauer, C. A.; Bhakta, R. K.; Louk, R. J. T. *Chem. Soc. Rev.* **2009**, *38*, 1330.
- (39) Kurmoo, M. *Chem. Soc. Rev.* **2009**, *38*, 1353.
- (40) Murray, L. J.; Dinca, M.; Long, J. R. *Chem. Soc. Rev.* **2009**, *38*, 1294.
- (41) Li, J. R.; Kuppler, R. J.; Zhou, H. C. *Chem. Soc. Rev.* **2009**, *38*, 1477.
- (42) Couck, S.; Denayer, J. F. M.; Baron, G. V.; Remy, T.; Gascon, J.; Kapteijn, F. *J. Am. Chem. Soc.* **2009**, *131*, 6326.
- (43) Farrusseng, D.; Aguado, S.; Pinel, C. *Angew. Chem., Int. Ed.* **2009**, *48*, 7502.
- (44) Lee, J.; Farha, O. K.; Roberts, J.; Scheidt, K. A.; Nguyen, S. T.; Hupp, J. T. *Chem. Soc. Rev.* **2009**, *38*, 1450.
- (45) Corma, A.; García, H.; i Xamena, F. X. L. *Chem. Rev.* **2010**, *110*, 4606.
- (46) Alaerts, L.; Seguin, E.; Poelman, H.; Thibault-Starzyk, F.; Jacobs, P. A.; de Vos, D. E. *Chem.—Eur. J.* **2006**, *12*, 7353.
- (47) Schlichte, K.; Kratzke, T.; Kaskel, S. *Microporous Mesoporous Mater.* **2004**, *73*, 81.
- (48) Horcajada, P.; Surble, S.; Serre, C.; Hong, D. Y.; Seo, Y. K.; Chang, J. S.; Greneche, J. M.; Margiolaki, I.; Férey, G. *Chem. Commun.* **2007**, 2820.
- (49) Gascon, J.; Hernandez-Alonso, M. D.; Ameida, A. R.; van Klink, G. P. M.; Kapteijn, F.; Mul, G. *J. Catal.* **2009**, *261*, 75.
- (50) Savonnet, M.; Aguado, S.; Ravon, U.; Bazer-Bachi, D.; Lecocq, V.; Bats, N.; Pinel, C.; Farrusseng, D. *Green Chem.* **2009**, *11*, 1729.
- (51) Hayashi, H.; Cote, A. P.; Furukawa, H.; O’Keeffe, M.; Yaghi, O. M. *Nat. Mater.* **2007**, *6*, 501.
- (52) Jhung, S. H.; Lee, J. H.; Yoon, J. W.; Serre, C.; Férey, G.; Chang, J. S. *Adv. Mater.* **2007**, *19*, 121.



- (53) Hwang, Y. K.; Hong, D. Y.; Chang, J. S.; Jhung, S. H.; Seo, Y. K.; Kim, J.; Vimont, A.; Daturi, M.; Serre, C.; Férey, G. *Angew. Chem., Int. Ed.* **2008**, *47*, 4144.
- (54) Sabo, M.; Henschel, A.; Froede, H.; Klemm, E.; Kaskel, S. *J. Mater. Chem.* **2007**, *17*, 3827.
- (55) Hermes, S.; Schröder, F.; Amirjalayer, S.; Schmid, R.; Fischer, R. A. *J. Mater. Chem.* **2006**, *16*, 2464.
- (56) Hermes, S.; Schroter, M. K.; Schmid, R.; Khodeir, L.; Muhler, M.; Tissler, A.; Fischer, R. W.; Fischer, R. A. *Angew. Chem., Int. Ed.* **2005**, *44*, 6237.
- (57) Schröder, F.; Esken, D.; Cokoja, M.; Van den Berg, M. W. E.; Lebedev, O. I.; Van Tendeloo, G.; Walaszek, B.; Buntkowsky, G.; Limbach, H. H.; Chaudret, B.; Fischer, R. A. *J. Am. Chem. Soc.* **2008**, *130*, 6119.
- (58) Muller, M.; Lebedev, O. I.; Fischer, R. A. *J. Mater. Chem.* **2008**, *18*, 5274.
- (59) Opelt, S.; Turk, S.; Dietzsch, E.; Henschel, A.; Kaskel, S.; Klemm, E. *Catal. Commun.* **2008**, *9*, 1286.
- (60) Ishida, T.; Nagaoka, M.; Akita, T.; Haruta, M. *Chem.—Eur. J.* **2008**, *14*, 8456.
- (61) Muller, M.; Hermes, S.; Kaehler, K.; Van den Berg, M. W. E.; Muhler, M.; Fischer, R. A. *Chem. Mater.* **2008**, *20*, 4576.
- (62) Henschel, A.; Gedrich, K.; Kraehnert, R.; Kaskel, S. *Chem. Commun.* **2008**, 4192.
- (63) El-Shall, M. S.; Abdelsayed, V.; Rahman, A. E.; Khder, S.; Hassan, H. M. A.; El-Kaderi, H. M.; Reich, T. E. *J. Mater. Chem.* **2009**, *19*, 7625.
- (64) Zlozea, C.; Campesi, R.; Cuevas, F.; Leroy, E.; Dibandjo, P.; Volkringer, C.; Loiseau, T.; Férey, G.; Latroche, M. *J. Am. Chem. Soc.* **2010**, *132*, 2991.
- (65) Pan, Y.; Yuan, B.; Li, Y.; He, D. *Chem. Commun.* **2010**, 46, 2280.
- (66) Yuan, B.; Pan, Y.; Li, Y.; Yin, B.; Jiang, H. *Angew. Chem., Int. Ed.* **2010**, *49*, 4054.
- (67) Férey, G.; Mellot-Draznieks, C.; Serre, C.; Millange, F.; Dutour, J.; Surblé, S.; Margiolaki, I. *Science* **2005**, *309*, 2040.
- (68) Küsgens, P.; Rose, M.; Senkovska, I.; Fröde, H.; Henschel, A.; Siegle, S.; Kaskel, S. *Microporous Mesoporous Mater.* **2009**, *120*, 325.
- (69) Huang, J. L.; Zhu, F. X.; He, W. H.; Zhang, F.; Wang, W.; Li, H. X. *J. Am. Chem. Soc.* **2010**, *132*, 1492.
- (70) van Attekum, P. M.; Th., M.; Trooster, J. M. *Phys. Rev. B* **1979**, *20*, 2335.
- (71) Gniewek, A.; Trzeciak, A. M.; Ziółkowski, J. J.; Kępiński, L.; Wrzyszczyński, J.; Tylus, W. *J. Catal.* **2005**, *229*, 332.
- (72) Voogt, E. H.; Mens, A. J. M.; Gijzeman, O. L. J.; Gens, J. W. *Surf. Sci.* **1996**, *350*, 21.
- (73) Cairns, G. R.; Cross, R. J.; Stirling, D. *J. Mol. Catal. A: Chem.* **2001**, *172*, 207.
- (74) Lebedev, O. I.; Millange, F.; Serre, C.; Van Tendeloo, G.; Férey, G. *Chem. Mater.* **2005**, *17*, 6525.
- (75) Ganesan, M.; Freemantle, R. G.; Obare, S. O. *Chem. Mater.* **2007**, *19*, 3464.
- (76) Ichikawa, S.; Poppa, H.; Boudart, M. *J. Catal.* **1985**, *9*, 1.
- (77) Fukuoka, A.; Sakamoto, Y.; Guan, S.; Inagaki, S.; Sugimoto, N.; Fukushima, Y.; Hirahara, K.; Iijima, S.; Ichikawa, M. *J. Am. Chem. Soc.* **2001**, *123*, 3373.
- (78) Consorti, C. S.; Flores, F. R.; Dupont, J. *J. Am. Chem. Soc.* **2005**, *127*, 12054.